

## Multiferroic and magnetoelectric properties of core-shell $\text{CoFe}_2\text{O}_4 @ \text{BaTiO}_3$ nanocomposites

Kalyan Raidongia,<sup>1</sup> Angshuman Nag,<sup>1,2</sup> A. Sundaresan,<sup>1</sup> and C. N. R. Rao<sup>1,2,a)</sup>

<sup>1</sup>Chemistry and Physics of Materials Unit, International Centre for Materials Science, CSIR Centre of Excellence in Chemistry, Jawaharlal Nehru Centre for Advanced Scientific Research, Jakkur P.O., Bangalore 560064, India

<sup>2</sup>Solid State and Structural Chemistry Unit, Indian Institute of Science, Bangalore 560012, India

(Received 14 June 2010; accepted 17 July 2010; published online 9 August 2010)

Core-shell  $\text{CoFe}_2\text{O}_4 @ \text{BaTiO}_3$  nanoparticles and nanotubes have been prepared using a combination of solution processing and high temperature calcination. Both the core-shell nanostructures exhibit magnetic and dielectric hysteresis at room temperature and magnetoelectric effect. The dielectric constant of both the nanocomposites decreases upon application of magnetic field. The core-shell nanoparticles exhibit 1.7% change in magnetocapacitance around 134 K at 1 T, while the core-shell nanotubes show a remarkable 4.5% change in magnetocapacitance around 310 K at 2 T. © 2010 American Institute of Physics. [doi:10.1063/1.3478231]

Zheng *et al.*<sup>1</sup> measured properties of nanofilms of  $\text{CoFe}_2\text{O}_4 @ \text{BaTiO}_3$ , where nanopillars of  $\text{CoFe}_2\text{O}_4$  were embedded in a  $\text{BaTiO}_3$  matrix and found a small change in magnetization at the ferroelectric transition temperature of  $\text{BaTiO}_3$ . Composites of  $\text{CoFe}_2\text{O}_4$  with  $\text{BaTiO}_3$  are reported to exhibit magnetoelectric effect by Doung *et al.*<sup>2</sup> and Wie *et al.*,<sup>3</sup> who suggest mechanical coupling between magnetostrictive and piezoelectric phases through magnetostriction to be responsible for the magnetoelectric effect. These workers did not, however, measure the magnetocapacitance as a function of applied magnetic field in these materials. Nanocomposites of  $\text{CoFe}_2\text{O}_4$  with  $\text{Pb}(\text{Zr}, \text{Ti})\text{O}_3$  show a very small magnetocapacitance (<0.1% at 1 T) at room temperature.<sup>4</sup> We considered it purposeful to investigate magnetic and dielectric properties of different types of core-shell nanostructures between  $\text{CoFe}_2\text{O}_4$  and  $\text{BaTiO}_3$  to explore the occurrence of magnetoelectric effect in these composites. For this purpose, we have prepared  $\text{CoFe}_2\text{O}_4 @ \text{BaTiO}_3$  core-shell nanoparticles as well as core-shell nanotubes.

$\text{CoFe}_2\text{O}_4$  nanoparticles (~12 nm diameter) were prepared by the hydrothermal treatment of a slurry obtained by reducing 15 mL aqueous mixture of  $\text{Co}(\text{NO}_3)_2 \cdot 6\text{H}_2\text{O}$  (0.058 g),  $\text{Fe}(\text{NO}_3)_3 \cdot 9\text{H}_2\text{O}$  (0.16 g), and polyvinylpyrrolidone (0.2 g) with sodium borohydride (0.9 g dissolved in 5 mL of millipore water) at 120 °C for 12 h.<sup>5</sup> We then prepared a precursor solution of  $\text{BaTiO}_3$  containing a mixture of 30 mL aqueous solution of 0.029 g of  $\text{BaCO}_3$  and 0.1 g of citric acid with 30 mL ethanolic solution of 1 g of citric acid and 0.048 mL titanium isopropoxide.  $\text{CoFe}_2\text{O}_4$  (0.1 g) nanoparticles were dispersed in 60 mL of the  $\text{BaTiO}_3$  precursor solution under vigorous sonication. After prolonged sonication, the mixture was dried at 60 °C under stirring and subsequently calcined at 780 °C for 5 h to obtain  $\text{CoFe}_2\text{O}_4 @ \text{BaTiO}_3$  core-shell nanoparticles. The diameter of these core-shell nanoparticles was between 40 and 60 nm, with the ferrite particles at the core [see the transmission electron microscopy (TEM) image in Fig. 1(a)] with an average thickness of  $\text{BaTiO}_3$  shell being ~18 nm.

$\text{CoFe}_2\text{O}_4$  nanotubes with an outer diameter of ~80 nm [see the TEM image in the inset of Fig. 1(b)] were obtained by using polycarbonate membrane templates with a pore diameter of 220 nm. The templates were soaked overnight in a 20 mL ethylene glycol solution containing 0.047 g of  $\text{CoCl}_2 \cdot 6\text{H}_2\text{O}$  and 0.109 g of  $\text{FeCl}_3 \cdot 6\text{H}_2\text{O}$  followed by drying at 120 °C and calcination at 530 °C for 3 h. These nanotubes were added into 10 mL of the  $\text{BaTiO}_3$  precursor solution, sonicated for five minutes and dried at 60 °C. The dried mixture was subsequently calcined at 780 °C for 5 h to obtain  $\text{CoFe}_2\text{O}_4 @ \text{BaTiO}_3$  core-shell nanotubes. A TEM image of  $\text{CoFe}_2\text{O}_4 @ \text{BaTiO}_3$  core-shell nanotubes with a diameter of around 100 nm is shown in Fig. 1(b). X-ray diffraction and selected area electron diffraction patterns of the core-shell nanostructures showed them to be mixtures of cubic  $\text{CoFe}_2\text{O}_4$  and tetragonal  $\text{BaTiO}_3$ . The particle size of  $\text{BaTiO}_3$  here was considerably small (~15 nm). Raman spectra confirmed the presence of tetragonal  $\text{BaTiO}_3$  with bands at 308, 520, and 718  $\text{cm}^{-1}$ .<sup>6</sup>

$\text{CoFe}_2\text{O}_4$  nanoparticles showed a large divergence between field cooled (FC) and zero field cooling (ZFC) magnetization data (obtained using PPMS from Quantum design, USA) in the 10–390 K range at 100 Oe, the divergence in-

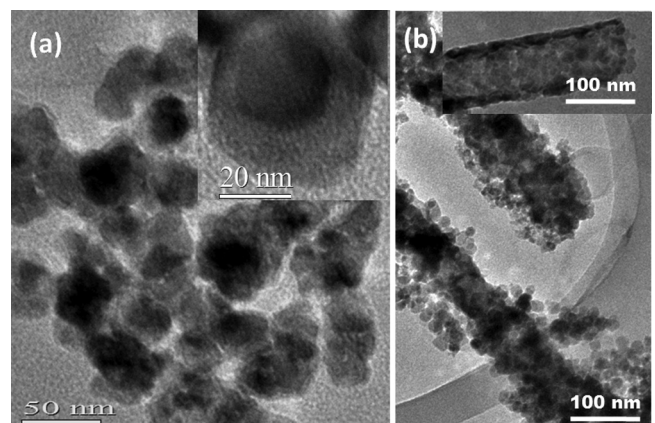


FIG. 1. TEM images of  $\text{CoFe}_2\text{O}_4 @ \text{BaTiO}_3$  core-shell (a) nanoparticles and (b) nanotubes. TEM image of a core-shell nanoparticle is shown in the inset of Fig. 1(a). Inset in Fig. 1(b) shows TEM image of a  $\text{CoFe}_2\text{O}_4$  nanotube.

<sup>a)</sup>Electronic mail: cnrrao@jncasr.ac.in.

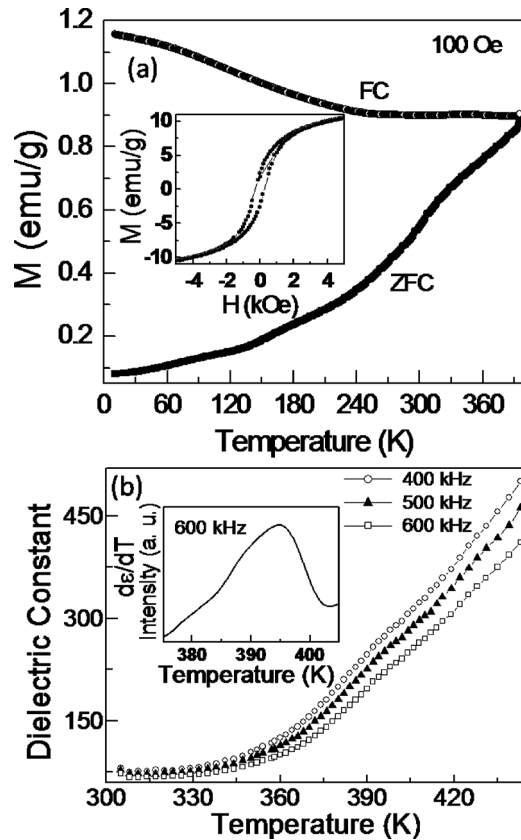


FIG. 2. (a) Temperature dependence of the magnetization of  $\text{CoFe}_2\text{O}_4@ \text{BaTiO}_3$  core-shell nanoparticles under FC and ZFC conditions. Inset shows the magnetic hysteresis at 300 K. (b) Temperature dependence of dielectric constant of  $\text{CoFe}_2\text{O}_4@ \text{BaTiO}_3$  core-shell nanotubes. Inset shows derivative of the dielectric constant to demonstrate the transition at 396 K.

creasing with decreasing temperature.<sup>5,7</sup> A similar behavior was found with the  $\text{CoFe}_2\text{O}_4$  nanotubes. Both the  $\text{CoFe}_2\text{O}_4$  nanoparticles and nanotubes exhibit magnetic hysteresis at 300 K. The saturation magnetization ( $M_s$ ), remanent magnetization ( $M_r$ ), and coercive field ( $H_c$ ) were 60 emu/g, 12 emu/g, and 166 Oe, respectively, in the case of  $\text{CoFe}_2\text{O}_4$  nanoparticles, values which are smaller than the bulk values as expected.<sup>8</sup> The  $M_s$ ,  $M_r$ , and  $H_c$  values of  $\text{CoFe}_2\text{O}_4$  nanotubes (outer diameter  $\sim 80$  nm) were 75 emu/g, 28 emu/g, and 901 Oe, respectively.

$\text{CoFe}_2\text{O}_4@ \text{BaTiO}_3$  core-shell nanoparticles at 100 Oe reveal divergence between the FC and ZFC magnetization data [Fig. 2(a)] just as the  $\text{CoFe}_2\text{O}_4$  nanoparticles. The ZFC plot also shows a shoulder around 140 K similar to the feature reported in the literature.<sup>7</sup> The core-shell nanoparticles also show magnetic hysteresis at 300 K [see inset of Fig. 2(a)], the  $M_s$  and  $M_r$  values being 13 and 2.4 emu/g these values are lower than those of pure  $\text{CoFe}_2\text{O}_4$  nanoparticles (the  $M_s$  and  $M_r$  values of the core-shell nanoparticles calculated on the basis of the weight of  $\text{CoFe}_2\text{O}_4$  alone are 20 emu/g and 4 emu/g, respectively). The coercive field, however, increases to 264 Oe in the core-shell particles, probably because the magnetization become harder in the presence of nonmagnetic shell.<sup>9</sup>

Temperature-dependence of the dielectric constant of  $\text{CoFe}_2\text{O}_4@ \text{BaTiO}_3$  core-shell nanoparticles was measured at different frequencies (1 kHz to 1 MHz) using precision impedance analyzer (Agilent 4294A). The dielectric constant

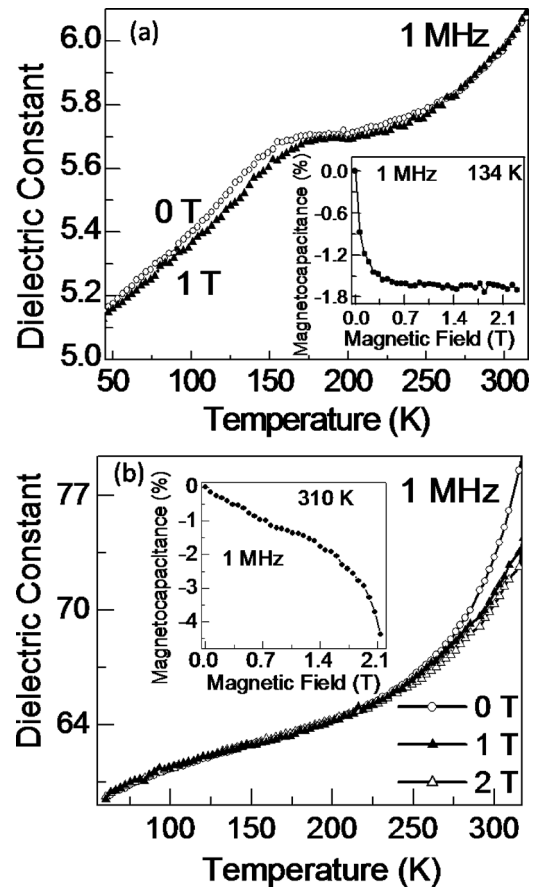


FIG. 3. Temperature variation in dielectric constant of  $\text{CoFe}_2\text{O}_4@ \text{BaTiO}_3$  core-shell (a) nanoparticles and (b) nanotubes at different magnetic fields. Insets in Figs. 3(a) and 3(b) show the magnetocapacitance as a function of magnetic field at 134 K and 310 K for the core-shell nanoparticles and nanotubes, respectively.

increases with increasing temperature with a clear hump at  $\sim 390$  K corresponding to the ferroelectric  $T_c$  of bulk  $\text{BaTiO}_3$  [see Fig. 2(b) for typical dielectric behavior]. The dielectric constant increases with decreasing frequency but the  $T_c$  does not change significantly with frequency.  $\text{BaTiO}_3$  nanoparticles (diameter  $\sim 20$  nm) as well as  $\text{CoFe}_2\text{O}_4@ \text{BaTiO}_3$  core-shell nanoparticles do not exhibit good dielectric hysteresis loops showing saturation. The instability of the ferroelectric phase depends on factors such as smaller grain size, defect chemistry, incorporation of  $\text{CoFe}_2\text{O}_4$ , presence of hydroxyl groups, aggregation of particles, porosity level, and residual stresses and it is difficult to separate one effect from another.<sup>10,11</sup> From the available data, we find that the coercive polarization ( $P_c$ ) and remnant polarization ( $P_r$ ) to be 51 kV/cm and 0.13  $\mu\text{C}/\text{cm}^2$ , respectively, for  $\text{BaTiO}_3$  nanoparticles, the corresponding values for core-shell nanoparticles being 13 kV/cm and 0.02  $\mu\text{C}/\text{cm}^2$ , respectively. Figure 3(a) shows the temperature dependence of the dielectric constant in the temperature range of 45–315 K in the absence and presence of 1 T magnetic field. Both the curves show a transition around 170 K which corresponds to the rhombohedral-orthorhombic phase transition ( $T_{ro}$ ) of  $\text{BaTiO}_3$ .<sup>12</sup> A decrease in the dielectric constant is observed below  $T_{ro}$  on application of the magnetic field, showing the presence of magnetoelectric effect in the core-shell structure. The inset of Fig. 3(a) shows the magnetocapacitance of the sample as a function of magnetic field at

134 K. The magnetocapacitance decreases with increasing magnetic field till 0.5 T accounting for  $\sim 1.7\%$  change but is independent of frequency.

We have studied properties of  $\text{CoFe}_2\text{O}_4@ \text{BaTiO}_3$  core-shell nanotubes as well, since the nanotubes exhibit large  $M_s$  and  $M_r$  compared to the nanoparticles, at the same time providing large interfacial area between  $\text{CoFe}_2\text{O}_4$  and  $\text{BaTiO}_3$  nanostructures. Magnetization data of the  $\text{CoFe}_2\text{O}_4@ \text{BaTiO}_3$  core-shell nanotubes also reveal divergence between FC and ZFC plots similar to the core-shell nanoparticles. We observe magnetic hysteresis at 300 K with  $M_s$  and  $M_r$  values of 28 and 12 emu/g, respectively, (the  $M_s$  and  $M_r$  values corresponding to the weight percent contribution of  $\text{CoFe}_2\text{O}_4$  core alone are 40 emu/g and 16 emu/g, respectively). The decrease in magnetization of  $\text{CoFe}_2\text{O}_4$  in the core-shell structures could be due to magnetostriction<sup>1,4</sup> as well as lattice mismatch with  $\text{BaTiO}_3$ .<sup>1</sup> Similar reduction in magnetic moment has been observed in the case of  $\text{CoFe}_2\text{O}_4$  dispersed in a  $\text{PbTiO}_3$  matrix due to the dissolution of Ti in the interface.<sup>13,14</sup> The  $H_c$  of the core-shell nanotubes is 912 Oe, comparable to that of pure  $\text{CoFe}_2\text{O}_4$  nanotubes.

Temperature variation in the dielectric constant of the core-shell nanotubes shows a transition at 396 K corresponding to tetragonal to cubic phase transition<sup>12</sup> of  $\text{BaTiO}_3$  [see Fig. 2(b)]. The  $P_c$  and  $P_r$  values obtained from the dielectric hysteresis of the core-shell nanotubes are 185 kV/cm and  $0.24 \mu\text{C}/\text{cm}^2$ , respectively, values larger than those of the nanoparticles. Figure 3(b) shows the temperature variation in the dielectric constant at low temperatures on application of a magnetic field. The dielectric constant decreases with increase in magnetic field above 270 K, close to the orthorhombic to tetragonal phase transition temperature. The magnetocapacitance of core-shell nanotubes at 310 K is shown as a function of magnetic field in the inset of Fig. 3(b). The magnetocapacitance decreases monotonically with increasing magnetic field till 2.1 T, exhibiting a substantial change of 4.5%. The 4.5% change in magnetocapacitance for core-shell nanotubes found here is a significant improvement over that of the core-shell nanoparticles (1.7%) and is the highest value reported so far in the  $\text{CoFe}_2\text{O}_4\text{-BaTiO}_3$  system. Furthermore, magnetocapacitance is independent of the frequency of measurement. The maximum magnetocapacitance is observed at different structural transition temperatures of

$\text{BaTiO}_3$  for the nanoparticles and nanotubes. This may be because the magnetic moment is high in the different temperature regimes in the case of nanoparticles and nanotubes, the temperature being low (134 K) in the case of former. Furthermore, the smaller size of the  $\text{BaTiO}_3$  nanoparticles on the  $\text{CoFe}_2\text{O}_4$  nanotubes may wipe out the 170 K transition.

In conclusion, core-shell  $\text{CoFe}_2\text{O}_4@ \text{BaTiO}_3$  nanoparticles and nanotubes exhibit magnetic hysteresis at room temperature and show magnetoelectric effect. The results obtained with core-shell nanotubes are noteworthy since we observe a 4.7% change in magnetocapacitance at 310 K. The larger change in magnetocapacitance of the core-shell nanotubes may arise from the larger saturation magnetization and remanent magnetization of the nanotubes.

K.R. acknowledges CSIR, India, for a fellowship and A.N. acknowledges IISc for a centenary postdoctoral fellowship.

- <sup>1</sup>H. Zheng, J. Wang, S. E. Lofland, Z. Ma, L. Mohaddes-Ardabili, T. Zhao, L. Salamanca-Riba, S. R. Shinde, S. B. Ogale, F. Bai, D. Viehland, Y. Jia, D. G. Schlom, M. Wuttig, A. Roytburd, and R. Ramesh, *Science* **303**, 661 (2004).
- <sup>2</sup>G. V. Duong and R. Groessinger, *J. Magn. Magn. Mater.* **316**, e624 (2007).
- <sup>3</sup>J. Nie, G. Xu, Y. Yang, and C. Cheng, *Mater. Chem. Phys.* **115**, 400 (2009).
- <sup>4</sup>X. Gao, B. J. Rodriguez, L. Liu, B. Birajdar, D. Pantel, M. Ziese, M. Alexe, and D. Hesse, *ACS Nano* **4**, 1099 (2010).
- <sup>5</sup>Z. Gu, X. Xiang, G. Fan, and F. Li, *J. Phys. Chem. C* **47**, 18459 (2008).
- <sup>6</sup>P. K. Dutta, P. K. Gallagher, and J. Twut, *Chem. Mater.* **5**, 1739 (1993).
- <sup>7</sup>Z. Wang, X. Liu, M. Lv, P. Chai, Y. Liu, X. Zhou, and J. Meng, *J. Phys. Chem. C* **112**, 15171 (2008).
- <sup>8</sup>M. Grigorova, H. J. Blythe, V. Rusanov, V. Petkov, V. Masheva, D. Nihtianova, L. M. Martinez, J. S. Munoz, and M. Mikhov, *J. Magn. Magn. Mater.* **183**, 163 (1998).
- <sup>9</sup>H. F. Zhang, S. W. Or, and H. L. W. Chan, *Mater. Res. Bull.* **44**, 1339 (2009).
- <sup>10</sup>U. A. Joshi, S. Yoon, S. Baik, and J. S. Lee, *J. Phys. Chem. B* **110**, 12249 (2006).
- <sup>11</sup>E. K. Akdogan, M. R. Leonard, and A. Safari, in *Handbook of Low and High Dielectric Constant Materials and Their Applications*, edited by H. S. Nalwa (Academic, New York, 1999), Vol. 2, p. 61.
- <sup>12</sup>C. Kittel, *Introduction to Solid State Physics*, 7th ed. (Wiley, New York, 1995).
- <sup>13</sup>J. Li, I. Levin, J. Slutsker, V. Provenzano, P. K. Schenck, R. Ramesh, J. Ouyang, and A. L. Roytburd, *Appl. Phys. Lett.* **87**, 072909 (2005).
- <sup>14</sup>P. Nathwani and V. S. Darshane, *J. Phys. C* **21**, 3191 (1988).